

Millennial pulses of African dust and ITCZ shifts in the Eastern Equatorial Pacific

Received: 23 August 2024

Accepted: 30 May 2025

Published online: 01 July 2025

Danielle E. Schimmenti¹, Franco Marcantonio¹✉, M. Roxana Sierra-Hernández² & Matthew W. Schmidt³

We present high-resolution records of detrital Pb and Nd isotopes from marine core site MV1014-02-17JC (00° 10.8297'S, 85° 52.0042'W) in the Eastern Equatorial Pacific (EEP) and use a Bayesian isotope mixing model, MixSIAR, to quantify global dust source contributions since the onset of the last glaciation 30,000 yr ago. We find that in addition to South American dust from the Andean margin, North African dust from the Saharan desert makes up significant proportions of the EEP dust delivered to the site of study. The proportion of North African dust was significantly enhanced during the cold Northern Hemisphere stadials, Heinrich Stadial 1 and the Younger Dryas, when dust fluxes were also higher. During the warm Bølling-Allerød and African Humid Periods, dust fluxes were decreased, and the proportion of South American dust was enhanced. We suggest the variability in the proportions of northern vs. southern hemisphere sourced dust in the EEP is indicative of large climate-related meridional shifts (>7°) in the average position of the Inter-tropical Convergence Zone, a major precipitation belt which, today, affects the lives of billions across our planet.

In the equatorial Pacific, dust provenance studies based on detrital Nd and Pb isotopic signatures of marine sediments represent a well-established method for reconstructing the average latitudinal position of the paleo-ITCZ^{1–4}, due to the ITCZ's role as a barrier to inter-hemispheric dust transport⁵ and the distinct Pb and Nd isotopic signatures (²⁰⁶Pb/²⁰⁴Pb, ²⁰⁷Pb/²⁰⁴Pb, ²⁰⁸Pb/²⁰⁴Pb and ϵ_{Nd}) of global dust sources. While these studies have established important constraints and hypotheses on ITCZ variability over the central equatorial Pacific (CEP) and westernmost EEP during the last and penultimate deglaciations, recent model simulations have shown that Pacific ITCZ responses to different climatic forcings are not zonally homogeneous and that some of the largest meridional shifts of the ITCZ are observed in the easternmost EEP during abrupt climate events⁶. There is therefore a need for millennial-scale resolution reconstructions of paleo-ITCZ variability further east in the basin. Here others have shown there to be changing patterns of export production that may be related to changes in the fluxes of CO₂ into and out of the ocean on climate timescales (e.g., Schimmenti et al.⁷, and references therein).

To date, South American volcanic systems from the Andean margin and loess from the deserts of China and Mongolia have been recognized as the prevailing northern and southern endmembers, respectively, of atmospheric dusts reaching the equatorial Pacific at 110°W and further west in the CEP^{1–3}. Modern dust trajectory models indicate that East Asian dust does not reach east of ~110°W in the equatorial Pacific and that instead, North Africa is the only possible northern hemisphere dust endmember that can physically reach the easternmost EEP (EEEP; east of 110°W). Due to the position of the ITCZ over the region, these models (e.g., ref. 8) estimate ~90–100% of the EEEP atmospheric dust load at the equator is South American in origin and ~10% or less is North African in origin today. However, the latter proportion increases to as much as 20–30% towards the north of the equator and particularly, the ITCZ at 7°N⁸. Beyond these model projections, there have yet to be any studies to 1) corroborate the presence of North African dust in the EEEP and 2) evaluate the proportions of Northern Hemisphere (North African) vs. Southern Hemisphere (South American)-sourced dust delivered to the region during the last

¹Department of Geology and Geophysics, Texas A&M University, College Station, TX, USA. ²Byrd Polar and Climate Research Center, The Ohio State University, Columbus, OH, USA. ³Department of Ocean and Earth Sciences, Old Dominion University, Norfolk, VA, USA. ✉e-mail: marcantonio@tamu.edu

30 kyr. This is best achieved through direct measurements of the isotope geochemistry of the fine-grained dust fraction of marine sediments, which is the aim of this paper.

Here we present new high-resolution records of detrital Nd and Pb isotopes from site MV1014-02-17JC (00° 10.8297'S, 85° 52.0042'W; see Fig. 1) in the Panama Basin. High-resolution dust fluxes to this core have already been reconstructed⁹. Here, working on the same samples analyzed for dust fluxes in Loveley et al.⁸, we reconstruct the provenance of the dust by compiling a database of the most likely potential dust source areas (PSAs) from around the globe based on available global projections, prevailing wind trajectories, and existing geochemical data (see “compilation of dust source data” section in Methods). We then execute two isotope ($^{206}\text{Pb}/^{204}\text{Pb}$ - ϵ_{Nd} and $^{208}\text{Pb}/^{204}\text{Pb}$ - ϵ_{Nd}) Bayesian mixing envelope analyses and mixing models (MixSIAR)^{10–12} with the Pb and Nd isotopic data from 17JC and our PSA database to identify the most geochemically probable PSAs and quantify their contributions to our site's dust load over time. We utilize these model results to constrain meridional shifts in the ITCZ for the EEP over the past 30,000 yr. The sub-millennial resolution of our records allows us to evaluate dust provenance and ITCZ change over abrupt climate events since the Last Glacial Maximum (LGM; 19–21 ka), at Heinrich Stadial 1 (HS1; 14.6–18 ka^{13,14}), the Bølling-Allerød (B/A; 14.6–13.6 ka¹⁵), the Younger Dryas (YD; 13.6–11.7 ka^{15,16}), and the Early Holocene/African Humid Period (EH/AHP; 11–5 ka¹⁷) in the equatorial Pacific. Importantly, because the timing of the shifts has been suggested to be related to changing patterns of export production in the EEP^{7,9,18}, clues to the relationship between the sources of dust delivery and atmospheric CO₂ levels may be discerned.

Results and discussion

Dust sources to the EEP over the past 30,000 years

In their reconstruction of dust fluxes over the last 30,000 years at this equatorial site, Loveley et al.⁹ found that, on average, during the last glacial, dust fluxes were higher than those in the Holocene by a factor of about two. Punctuated throughout this longer-term climatic relationship were pulses of high dust fluxes during HS1, and at the LGM (~20 kyr). Dust fluxes decreased during the B/A but then stalled during the YD, until continuing their decrease again during the EH/AHP (lowest dust fluxes measured in the record). Using Pb and Nd isotope ratios, our goal here is to determine the sources of the dust delivered to the EEP at our site during each of these climatic intervals.

There is considerable variability in detrital $^{206}\text{Pb}/^{204}\text{Pb}$, $^{208}\text{Pb}/^{204}\text{Pb}$, and ϵ_{Nd} over the past 30 kyr at 17JC (Fig. 2). We note $^{206}\text{Pb}/^{204}\text{Pb}$ and $^{208}\text{Pb}/^{204}\text{Pb}$ are most radiogenic (highest) during the LGM and

HS1 and least radiogenic at the YD and pre-HS1. For ϵ_{Nd} , values are least radiogenic (more negative) during the LGM, HS1, and YD and more radiogenic during the B/A and Early Holocene. Dust trajectory models indicate that the two major dust sources to this corner of the EEP today are South America and North Africa (e.g., refs. 8,19). The range of $^{206}\text{Pb}/^{204}\text{Pb}$ and $^{208}\text{Pb}/^{204}\text{Pb}$ at 17JC (Supplementary Data Table 1) is consistent with a South American dust source endmember to the equatorial Pacific as has been established in the CEP and further west of our site at 110°W^{2,4,20}. These young volcanic sources cannot, however, explain the significantly unradiogenic ϵ_{Nd} values in the 17JC detrital record (Supplementary Data Table 1), which are indicative of mixing with older continental material. The two candidates for this older continental material are North Africa and Asia. Models consistently rule out the ability for Asian dust sources (e.g., Chinese loess) to reach east of 110°W⁸. Instead, we suggest here that the older continental material represented by detrital unradiogenic Nd isotope ratios (and radiogenic Pb isotope ratios) are derived from North African dust sources most distinctly during HS1 and the early YD.

To determine the predominant mixtures of dust sources to 17JC, we first consider and compile all possible North African and South American PSAs to the EEP^{21–26} (see Methods for complete description of PSAs). We find that 17JC detrital data are best captured in $^{206}\text{Pb}/^{204}\text{Pb}$ - ϵ_{Nd} and $^{208}\text{Pb}/^{204}\text{Pb}$ - ϵ_{Nd} space by 11 PSAs from across North Africa²⁶ and the Andean margin of South America^{21–25} that include: the West African Coast (PSA-WAC), Mali Center (PSA-MC), the Bodele depression (PSA-BD), Libya Algeria Mali (PSA-LAM), Libya Egypt (PSA-LE), North, Middle and Southern Central Western Argentina (CWA), the Puna, the Altiplano, and the Paracas High (data for each PSA are reproduced in the Supplementary Data Table 7). After choosing the PSAs we use the Bayesian isotope mixing model, MixSIAR^{10,11}, to justify our choices (see Methods). Briefly, we first statistically validate that our 17JC Pb and Nd isotope data are enveloped by the mean Pb and Nd isotope signatures of the PSAs (Supplementary Fig. 1). We run Bayesian mixing polygon simulations of the $^{206}\text{Pb}/^{204}\text{Pb}$ - ϵ_{Nd} and $^{208}\text{Pb}/^{204}\text{Pb}$ - ϵ_{Nd} systems with data from the 11 PSAs and the 17JC detrital data^{11,12} (see Methods and Supplementary Figs. 1 and 2). On average, we find that there is a 95% chance that the 17JC detrital data fall within the two-dimensional mixing polygon formed by the PSA dataset in $^{206}\text{Pb}/^{204}\text{Pb}$ - ϵ_{Nd} space and about an 80% chance within $^{208}\text{Pb}/^{204}\text{Pb}$ - ϵ_{Nd} space (Supplementary Fig. 2). We proceed with the construction of our isotope mixing models based on our analysis that, in these two isotope systems, we have captured the majority of the endmembers for the full 30,000-year detrital record at 17JC.

To quantify the contributions of each of the 11 PSAs from South America and North Africa to the dust load at 17JC through time, we construct two two-isotope ($^{206}\text{Pb}/^{204}\text{Pb}$ - ϵ_{Nd} and $^{208}\text{Pb}/^{204}\text{Pb}$ - ϵ_{Nd})

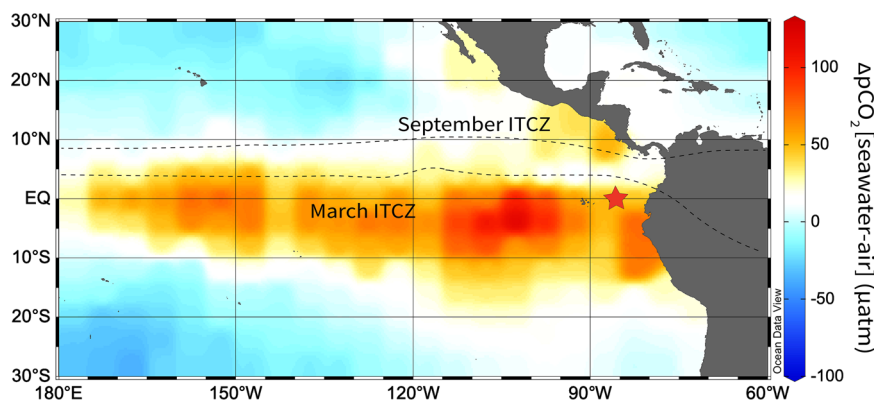


Fig. 1 | Location map for area of study. $\Delta p\text{CO}_2$ [seawater-air] flux from Takahashi et al.⁴⁸ with location of study site MV1014-02-17JC (red star) and the maximum (September) and minimum (March) mean seasonal positions of the Intertropical

Convergence Zone (ITCZ, black dashed lines)²⁵. Figure modified from Schimmenti et al.⁷. Source data are provided as a Source Data file in the supplemental section.

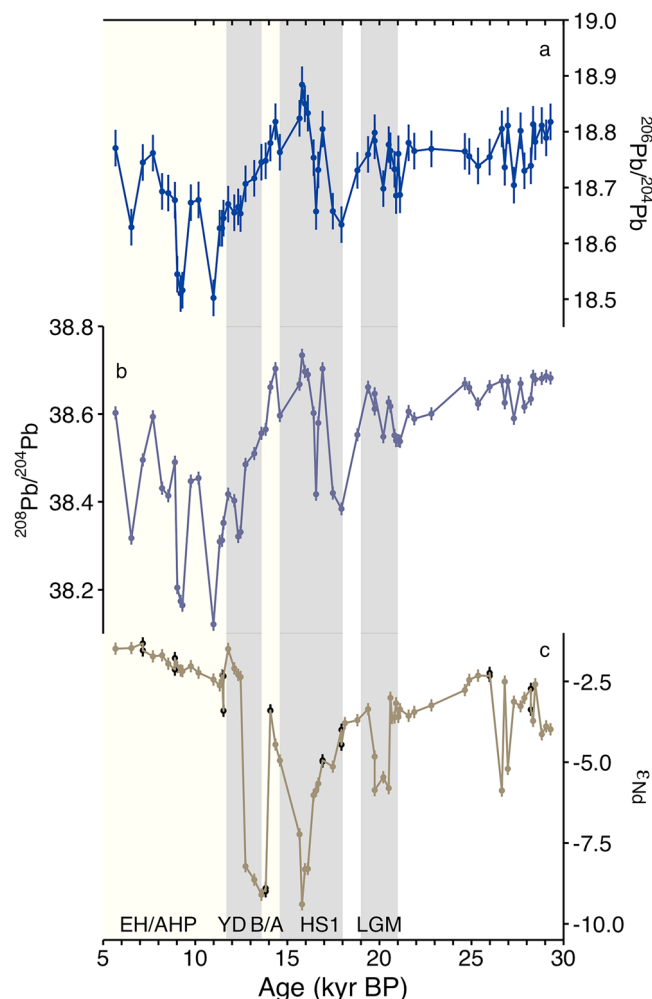


Fig. 2 | Detrital Pb and Nd isotope signatures at 17JC versus time over the past 30,000 yrs. **a** (top panel) $^{206}\text{Pb}/^{204}\text{Pb}$, **b** (middle panel) $^{208}\text{Pb}/^{204}\text{Pb}$, **c** (bottom panel) ϵ_{Nd} . Cold periods (Last Glacial Maximum-LGM, Heinrich Stadial-HS1, Younger Dryas-YD) are highlighted with gray bars and warm periods are highlighted with yellow bars (Bolling/Allerod-B/A and Early Holocene/African Humid Period-EH/AHP). Lines through data points represent error bars (see Methods). Black data points in panel (c) represent replicate measurements of ϵ_{Nd} (Supplementary Data Table 1). Source data are provided as a Source Data file in the supplemental section.

Bayesian mixing models with MixSIAR (see Methods). The results of the $^{206}\text{Pb}/^{204}\text{Pb} - \epsilon_{\text{Nd}}$ model are shown in Figs. 3 and 4. The results of the $^{208}\text{Pb}/^{204}\text{Pb} - \epsilon_{\text{Nd}}$ model, which are virtually the same, are shown in Supplementary Figs. 5 and 6. We find that the majority of the dust load at 17JC over the past 30,000 years can be attributed to contributions from South American PSAs (~75% on average; Fig. 3), with smaller contributions from North African PSAs (~25% on average; Fig. 3). The major South American sources over our record are the Paracas High and broadly, CWA, with lesser contributions from the Puna and Altiplano (Fig. 3a), whereas the relative contributions of the five North African PSAs are quite similar on average with larger variations occurring during discrete climate events such as HS1 and the YD (Fig. 4; *a posteriori* climate event grouping described further below).

To more fully consider the relationship between millennial climate events and changes in dust sources to the EEP, we performed *a posteriori* grouping of the model results by climate event (see Methods). We note significant and opposite variations in the contributions of South American vs. North African PSAs during abrupt cooling (HS1 and the YD) and warming events (the B/A and EH/AHP) of the deglaciation and early Holocene (Fig. 4). Furthermore, the contributions of

the South American PSAs decrease and those of the North African PSAs increase from the onset of the deglaciation during Marine Isotope Stage (MIS) 2 through the LGM and early deglacial, reaching a trough/peak (~30:70, North Africa:South America), respectively, at HS1 (Fig. 4). At HS1, the majority of South American dust is sourced from the Paracas High and the MCWA, with lesser contributions from the Altiplano, NCWA, and SCWA (Fig. 4a), whereas the majority of the North African dust is sourced from the Bodelé depression, Libya-Egypt, and Mali center with lesser contributions from Libya-Algeria-Mali, and the West African Coast (Fig. 4b). At the B/A, the proportion of South American vs. North African dust increases again (~80:20). There is a marked increase in the contribution of NCWA, smaller increases in that of the Paracas High and SCWA, slight decreases in the contributions of the Altiplano, and no significant change in the contribution of the Puna or MCWA PSAs (Fig. 4a). Contributions of all the North African PSAs decrease at the B/A, such that the largest contributions come from the Bodelé depression and Libya-Egypt with lesser contributions from PSA-MC followed by PSA-LAM and WAC (Fig. 4b). The proportion of North African dust to South American dust increases yet again at the YD (~30:70). Relative to the B/A, the contributions of PSA-WAC and PSA-LAM double, PSA-MC increases by 1.5-fold, and PSA-BD and LE remain largely the same (Fig. 4b), whereas the contributions of the Puna and NCWA decrease and that of the Altiplano and SCWA increase slightly (Fig. 4a). Finally, the onset of the EH and AHP are marked by elevated proportions of South American vs. North African dust (~85:15). This time, all North African PSA contributions, except for Libya-Egypt, are reduced to relatively equal proportions (Fig. 4b). The contributions of SCWA, MCWA, and the Paracas High increase at the onset of the EH whereas that of the Puna, Altiplano, and NCWA decrease slightly or remain constant (Fig. 4a).

Millennial migration of the mean position of the ITCZ in the EEP

Today, models suggest that ~20–25% and ~75–80% of the eolian dust deposited in the EEP near 17JC comes from North Africa and South America, respectively⁸. We have detrital Pb and Nd isotope ratio observational data to support these models. South American dust dominates the dust load to the equator because the ITCZ sits north of it and acts as an effective barrier to African dust (Figs. 3 and 4). Using our Nd-Pb isotope ratio mixing model results, from 30 kyr to the present, the proportion of dust from Africa increases and culminates with a significantly higher proportion during HS1. At the B/A, the proportion of African dust supplied to our site decreases before rapidly increasing again during the YD. After the YD, the proportion of African dust retreats to its lowest values in the early Holocene/AHP (Figs. 3 and 4). Each of these intervals of climate change associated with changes in the proportion of African to South American dust delivery likely signifies a considerable migration of the ITCZ since the onset of the last deglaciation 30,000 years ago.

We see evidence for a potential southward shift of the mean ITCZ relative to today at the LGM. During the LGM, 17JC dust is a mix of dust sourced from African and South American sources at an approximate proportion of 22:78 (Fig. 4). This contrasts with the lower proportions of African dust (relative to South American dust) delivered to our site during the Holocene (~15:85) (Fig. 4). This is in agreement with modeling studies^{6,27}, dust provenance records¹, and SST reconstructions^{28,29} over both the Atlantic and Pacific Oceans. This is also consistent with evidence from 17JC for reduced upwelling and therefore silica delivery/diatom productivity during the LGM due to the ITCZ shifting south, closer to the equator thus dampening cross-equatorial flow of the trade winds⁷. Notably, the proportion of African to South American dust deposited at 17JC does not appear to change after the LGM during the early deglaciation, suggesting the ITCZ may not have moved significantly from its LGM position. Hypotheses concerning changes in the mean position of the ITCZ in the Pacific Ocean, as shown here and by others^{1–4,7,9,18,20}, is in stark contrast to the Atlantic Ocean where there

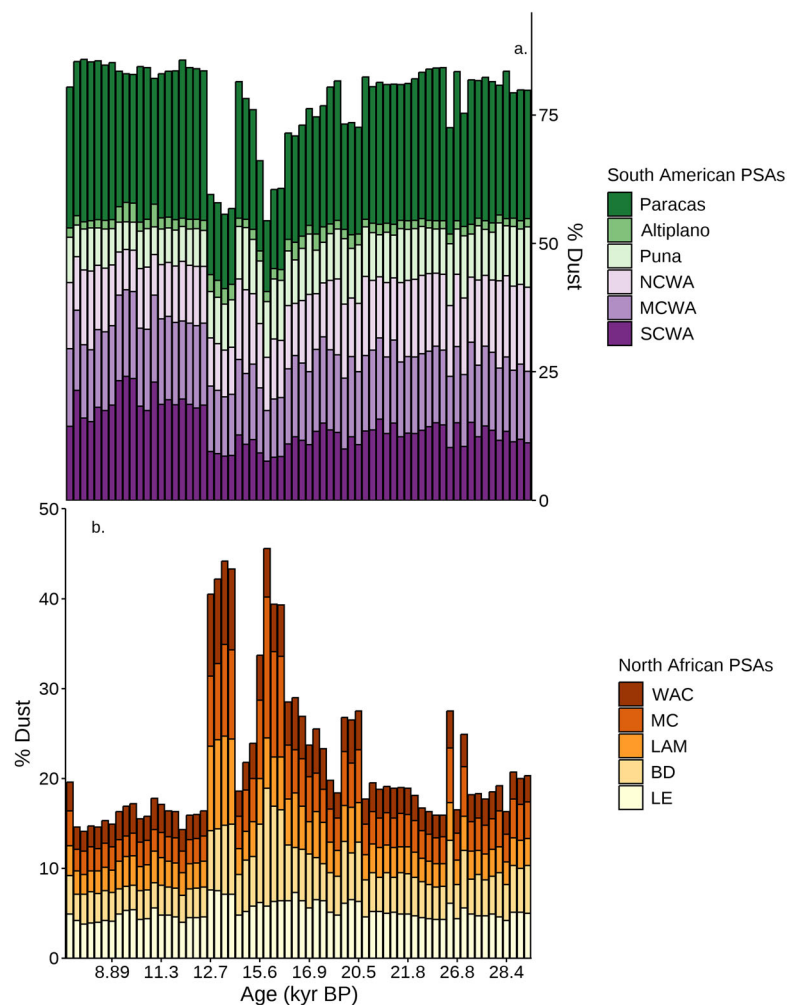


Fig. 3 | Provenance of 17JC dust in each sample over the past 30,000 years. Results from the $^{206}\text{Pb}/^{204}\text{Pb}$ - ϵ_{Nd} MixSIAR model. **a** % South American dust vs. time, color-coded by PSA. **b** % North African dust vs. time, color-coded by PSA. Sample

ages are plotted on a discrete scale on the x-axis. Source data are provided as a Source Data file in the supplemental section.

is little evidence for a shift in the mean position of the ITCZ on glacial-Holocene timescales³⁰.

At HS1 there is about a 30–40% increase in the proportion of African to South American dust relative to both the LGM and deglacial (ratio increases from about 22:78 to 30:70), indicative of a further southward shift of the ITCZ. Evidence for enhanced upwelling at 17JC⁷ and strengthened NE/ weakened SE trade winds²⁷ support the possibility of the ITCZ being further south during HS1 than during the LGM. Further, model simulations of the ITCZ, produce zonal mean and regional EEP ITCZ shifts that are greater under Heinrich Stadial-like forcings than LGM-like forcings⁶. The EEP ITCZ, specifically, exhibits southward shifts as large as 10° of latitude that are reproduced across all models for HS events; and most of the zonal mean shift of the ITCZ during HS events is due to shifts of the ITCZ over the CEP and EEP. We, therefore, favor a southward shift of the average position of the EEP ITCZ of at least 7° to a position south of the equator to produce the significant increase in African dust to the dust load that we observe at the equator at 17JC during HS1.

During the B/A, the proportion of African to South American dust delivered decreases to LGM levels (~20:80), suggesting a northward migration of the ITCZ. Given the similar proportions for LGM dust, we expect that the average latitudinal positions of the B/A and LGM ITCZs

were similar. This represents an improved constraint on the relative magnitude of ITCZ shift between HS1 and the B/A over the EEP, which was previously unclear from existing high-resolution records of Pacific ITCZ migrations over this timeframe^{7,31}.

At the YD, the proportion of African to South American dust is once again elevated (~30:70), suggesting a significant southward shift in the ITCZ like that interpreted for HS1. Similar to HS1, a strengthening of the NE trade winds/SE trade winds occurred with cooling and ITCZ displacement at the YD³². Upon closer examination, one might conclude that the smaller ratio of African to South American dust relative to HS1 at the YD (Fig. 4) indicates a smaller southerly displacement of the YD ITCZ relative to the HS1 ITCZ. However, there is evidence from the West African margin that this difference can be explained by latitudinal differences in peak northeasterly wind anomalies over North Africa between these two events¹⁶. In particular, the wind anomalies peak south of 20°N during HS1 and north of 20°N during the YD¹⁶. The dust provenance record at 17JC may be capturing these differences. At HS1, the increase in African dust is primarily driven by contributions from PSA-MC and PSA-BD, both of which lie south of 20°N, whereas at the YD peak African dust proportions are driven by elevated contributions from PSA-WAC and PSA-LAM (these increase while the contributions of PSA-BD, MC, and LE all decrease relative to that at

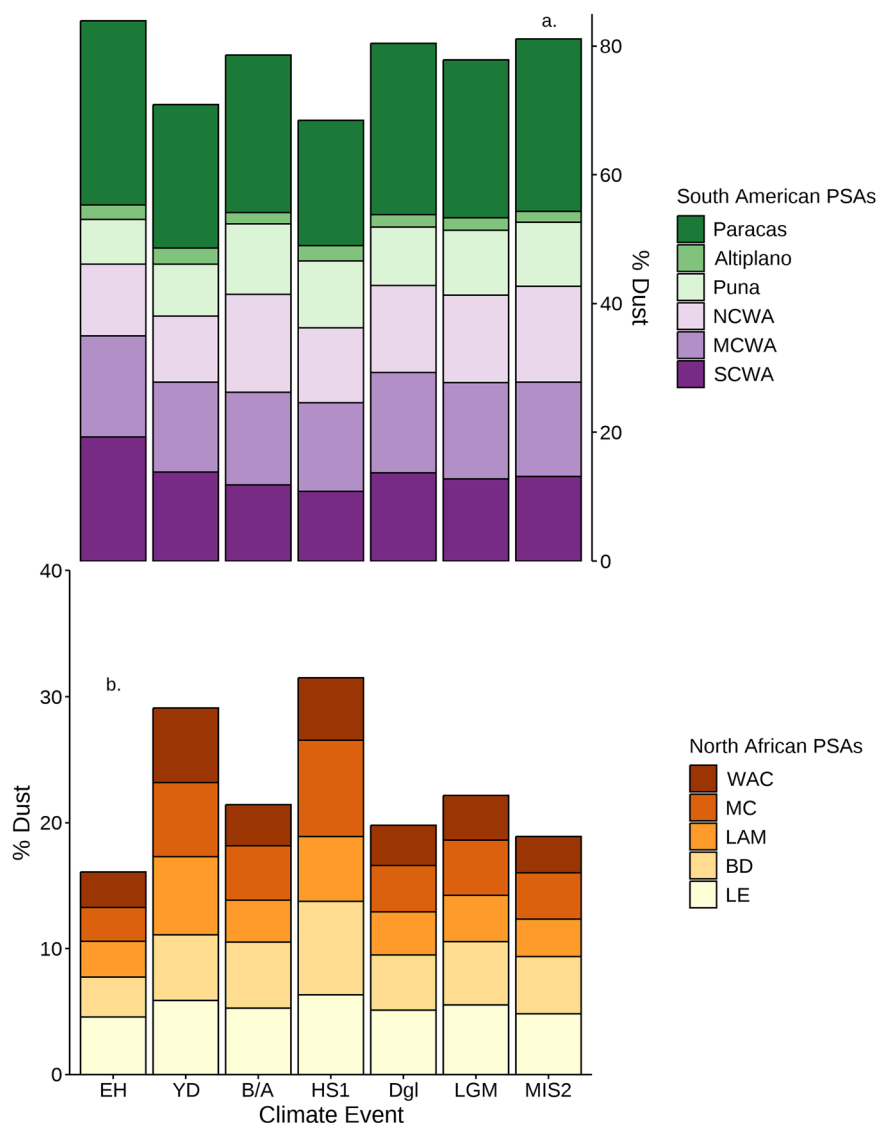


Fig. 4 | Provenance of 17JC dust during each climate event of the past 30,000 years. Results from the $^{206}\text{Pb}/^{204}\text{Pb}$ - ε_{Nd} MixSIAR model. **a** % South American dust vs. time, color-coded by PSA. **b** % North African dust vs. time, color-coded by PSA. MIS 2 Marine Isotope Stage 2, pre-LGM, LGM Last Glacial Maximum, Dgl

Deglacial, pre-HS1, HS1 Heinrich Stadial 1, B/A Bølling-Allerød, YD Younger Dryas, EH Early Holocene. Source data are provided as a Source Data file in the supplemental section.

HS1), both of which extend north of 20°N. We cannot unequivocally decipher relative differences in ITCZ position during the YD versus HS1 at this time, but our results are consistent with changes in the latitudinal placement of North African wind anomalies¹⁶.

Finally, during the Early Holocene, the lowest proportion of African to South American dust (-15:85) suggests the northernmost displacement of the ITCZ in our record. This is in agreement with evidence from 17JC for enhanced upwelling and silica delivery/diatom productivity (Pa/Th ratios, Fig. 4a in ref. 7) with strengthening of the SE trade winds and northward displacement of the ITCZ over the EEEP driven by peak boreal summer insolation at -10 ka⁷. The reduction in African dust is also consistent with evidence for intensification of the African monsoon and therefore enhanced precipitation and decreased aridity of the Sahara associated with the AHP.³³

To summarize, our observation-based Bayesian isotope mixing model suggests that dust delivered over the past 30,000 yr to the EEEP oscillates between delivery of varying proportions of dust sources from North Africa and South America. The shifts in the proportion of dust supplied from each continent can be explained by meridional shifts of the ITCZ in the eastern Pacific

Ocean across distinct climate events. Indeed, our work suggests southward shifts of the ITCZ during cold periods (LGM, HS1, and YD), with the most extreme shift of at least 7° during HS1 when the most significant proportion of African dust is apparent. Conversely, northward shifts of the ITCZ during warm climate events of the EH/AHP and B/A can be discerned based on the highest proportion of South American sources of dust delivered during these times. Overall, our radiogenic Pb and Nd isotope data on dust supply source changes provide the strongest evidence to date for significant migrations of the ITCZ over the EEEP during abrupt climate change events.

Methods

Site and sampling

Deep-sea sediment core MV1014-02-17JC (17JC) was retrieved from south of the Carnegie Ridge in the Panama Basin (00° 10.8297'S, 85° 52.0042'W; Fig. 1) at a water depth of 2846 m; just above the lysocline in this region³⁴. The average sedimentation rate at 17JC is 18 cm/kyr⁹ corresponding to an age resolution of -60–500 yr for an average sampling resolution of 3 cm downcore.

Age model

Using the Bayesian statistical package for age depth modeling ‘rbacon’³⁵ in R we extended the age model for the upper core (355 cm) at 17JC from Schimmenti et al.⁷ to the full core record (930 cm) with a combination of 21 radiocarbon ages (*N. duertrei*)^{7,9}, 5 tie points between Heinrich Stadial (HS) events in the 17JC ²³⁰Th MAR record⁹ and Hulu Cave³⁶, and ash from the Los Chocoyos eruption (75 ± 2 kyr)³⁷ identified at 853 cm in core 17JC (Supplementary Data Table 6). We ran bacon with a section thickness of 10 cm and an average accumulation rate of 90 yr cm^{-1} . Radiocarbon ages were calibrated to calendar year using the Marine20 calibration curve and its built-in 500-year reservoir age correction in bacon. Four thousand Markov Chain Monte Carlo (MCMC) iterations yielded a Gelman and Rubin Reduction Factor of 1.025, below the 1.05 safety threshold, indicating robust MCMC mixing for our model. Calibrated age errors were calculated by the model based on a 95% confidence interval, which yielded an average uncertainty for the calibrated radiocarbon ages of +469 years/–485 years and an average age model uncertainty of +683 years/–700 years (Supplementary Data Table 6) for the period of 5–30 ka.

Isolation of the detrital Nd and Pb

We measured the Nd and Pb isotopic composition of the operationally defined detrital fraction (the non-biogenic and non-authigenic component) of 17JC sediment, to best capture the signature of fine-grained eolian dust deposited over time at our site. To isolate the operationally defined detrital fraction, bulk sediment samples were wet-sieved to collect the $<63 \mu\text{m}$ fraction, then sequentially leached to remove carbonates, Fe-Mn oxyhydroxide coatings, and biogenic silica per the following procedure. ~500 mg of sediments ($<63 \mu\text{m}$) were dried down and homogenized, then sequentially leached with 10% buffered acetic acid, 0.02 M hydroxylamine hydrochloride with 25% acetic acid, and at 80 °C in a water bath with 2 M KOH. The detrital fraction was digested using a series of trace metal grade or distilled 8 N HNO₃, concentrated HF, concentrated H₂O₂, and aqua regia additions. Pb was eluted on anion exchange (AGIX8, 100–200 mesh) columns. Nd was eluted, after being washed off the Pb columns, through additional RE Spec (Eichrom) and Ln Spec (Eichrom) columns.

Nd and Pb isotope analysis

Nd and Pb isotope ratios were measured by Multi-Collector Inductively Coupled Mass Spectrometry (MC-ICP-MS) on a ThermoFisher Neptune Plus MC-ICP-MS in the Williams Radiogenic Laboratory at Texas A&M University. Approximately 200 ng Pb and Nd were analyzed per sample. Pb isotopes, expressed as the ratio of the radiogenic isotope (²⁰⁶Pb, ²⁰⁷Pb, or ²⁰⁸Pb) to the stable isotope (²⁰⁴Pb), were first corrected for instrumental mass bias using the exponential law through Tl addition. Samples and the NIST SRM 981 standard were spiked with 10 ng of Tl (NIST SRM 997). Data were internally mass-fractionation corrected using a ²⁰⁵Tl/²⁰³Tl ratio of 2.3889 based on the certified ratio of NIST SRM 997. An additional correction for sample Pb isotope ratios was then performed by bracketing every fourth sample with the NIST SRM 981 standard (and correcting to ²⁰⁶Pb/²⁰⁴Pb = 16.9406, ²⁰⁷Pb/²⁰⁴Pb = 15.497, ²⁰⁸Pb/²⁰⁴Pb = 36.7184; Yuan et al.³⁸).

Instrumental mass bias for Nd was corrected by first normalizing internally to a ¹⁴⁶Nd/¹⁴⁴Nd of 0.7219 after correcting for any Sm interferences. Sample ¹⁴³Nd/¹⁴⁴Nd ratios were then corrected by bracketing every three samples with the JNdi-1 standard (¹⁴³Nd/¹⁴⁴Nd = 0.512115 ± 0.0000007; Tanaka et al.³⁹). Nd isotopes ratios were normalized to the Nd isotopic composition of bulk earth obtained from chondrites by the following Eq. (1)⁴⁰:

$$\epsilon_{\text{Nd}} = \left(\frac{{}^{143}\text{Nd}}{{}^{144}\text{Nd}}_{\text{sample}} \bigg/ \frac{{}^{143}\text{Nd}}{{}^{144}\text{Nd}}_{\text{chondritic}} - 1 \right) 10^4 \quad (1)$$

Both NIST SRM 981 and JNdi-1 standards were analyzed within the same concentration range as the sample aliquots (5–25 ppb). 10 replicate samples were analyzed for Pb and Nd. The average reproducibility (2σ standard error) of the replicates for Pb were 0.03, 0.003, and 0.01 for ²⁰⁶Pb/²⁰⁴Pb, ²⁰⁷Pb/²⁰⁴Pb, and ²⁰⁸Pb/²⁰⁴Pb, respectively. Average external reproducibility (2σ standard error) of the JNdi-1 standards was 0.19 ε units. Procedural blanks were measured such that blank corrections were unnecessary.

Compilation of dust source data

Major dust sources to the EEP were chosen from the eight main global dust source regions following the work of Kok et al.⁸. Their model showed that the two main dust sources to the EEP east of the Galapagos today are South America and North Africa. Prospero et al.⁴¹ found that the main dust source areas on the South American continent broadly include the Bolivian Altiplano, Western Argentina, and Patagonia. More recent work by Gili et al.^{21,22} and Briceño-Zuluaga et al.⁴² refined the list of South American Potential Source Areas (PSAs) to five arid regions of the Andean margin extending from southern Peru to the tip of the continent: the Paracas High (Paracas; -13°–15°S), the Puna Altiplano Plateau (PAP; -15°–27°S), Central Western Argentina (CWA; -27°–38°S), Patagonia (-38°–52°S) and Tierra del Fuego (-53°–55°S). Based on prevailing winds, we limited South American PSAs to 17JC to those north of 38°S, as those south of this boundary should not physically reach the EEP and therefore should not contribute significantly to the South American dust budget at 17JC. This has been further corroborated by dust provenance studies that have shown Patagonia and Tierra del Fuego are significant sources of dust reaching the Southern Ocean and Antarctica^{21,22,43} and not the equatorial Pacific¹⁵.

Nd and Pb isotopic data for the Paracas High and PAP were obtained from Gili et al. (2016; 2017)^{21,22} and by filtering Central Volcanic Zone rock data from Mamani et al.²³ to the latitudinal and longitudinal ranges of the Paracas, Puna, and Altiplano, respectively²⁴. Puna and Altiplano data from Mamani et al.²³ were further filtered by sample/rock type to only include ignimbrites (South Puna and South Altiplano) and gneisses (North Puna) in order to best capture the isotopic signatures of the deflatable material from these PSAs, following the work of Gili et al.^{21,22}.

Nd and Pb isotopic data for CWA were obtained from Gili et al.^{21,22} and from the GEOROC database²⁴ (<https://georoc.eu/georoc>). Data from the latter database were downloaded on 16 May 2023 using the following parameters: geography = latitude 27°–38°S; longitude 65°–70°W; All samples: All types of material. This yielded mostly volcanic whole rock data from the Central and South Volcanic Zones (CVZ; SVZ) of the Andes. Gili et al.^{21,22} defined three regions of the CWA based on the rare earth and isotopic composition of deflatable material found there: the North CWA (NCWA; -27°–29°S), the Middle CWA (MCWA; -29°–33°S), and the South CWA (SCWA; -33°–36°S). NCWA and MCWA deflatable material are most similar in Nd and Sr isotopic composition to granitoids and metamorphic rocks of the Sierras Pampeanas whereas that of deflatable material from the SCWA is most similar to rocks of the Northern South Volcanic Zone (NSVZ; -33–36°S)³². Unfortunately, there is no Pb isotopic data available for Sierras Pampeanas granitoids and metamorphic rocks or NCWA/MCWA sediments. Consequently, we filtered our GEOROC CVZ/SVZ volcanic rock dataset to best match the latitudinal ranges and/or source areas of the CWA regions defined by Gili et al.^{21,22}, and which we named the following: NCWA_Volcanics (27°–29°S), Sierras Pampeanas (SP)_Volcanics (-31°S), and NSVZ-SCWA (33°–36°S).

North African PSAs and their isotopic signatures were taken from Guinoseau et al.²⁶. These authors divided the PSAs into several groups which include Libya-Algeria-Mali (PSA-LAM), Libya-Egypt (PSA-LE), the Bodélé Depression (PSA-BD), Mali Center (PSA-MC), and the West African Coast (PSA-WAC). Outliers in ²⁰⁶Pb/²⁰⁴Pb, ²⁰⁸Pb/²⁰⁴Pb, and ϵ_{Nd}

were identified for each South American PSA using Rosner's test in the EnvStats package in R¹² and removed from their respective datasets. Outlier identification and removal was performed by similar means for Pb and Nd isotope data of the North African PSAs by Guinoiseau et al.²⁶.

It is important to note that the PSA data from the literature may not represent perfectly the dust emitted from these areas and delivered to the eastern Pacific. For example, for Pb isotopes grain size sorting during dust transport may marginally influence the Pb isotope ratio²⁶. Nd isotopes are less likely to undergo a grain size fractionation effect during transport⁴⁴. When possible, we used only samples for which both Pb and Nd isotope ratios were measured for the detrital deflatable material in the source region. Although this was not always possible, our attempt at creating a database of PSAs is a good first estimate or starting point given the lack of detrital source data from the South American continent.

Isotope mixing models

The MixSIAR package in R^{10,11} was used to estimate the proportions of dust source contributions to the 17JC dust load through time, following the work of Longman et al.⁴⁵ Dietrich et al.⁴⁶ and Lopez et al.⁴⁷ on environmental Pb source modeling with Pb isotope ratios. Bayesian mixing polygon simulations^{10,11} were first run in R to determine which PSAs and which combination of Pb and/or Nd isotope ratios (²⁰⁶Pb/²⁰⁴Pb, ²⁰⁷Pb/²⁰⁴Pb, ²⁰⁸Pb/²⁰⁴Pb, ϵ_{Nd}) best explained the isotopic signature of 17JC data. The results of these simulations were then used to construct two two-isotope models using ²⁰⁶Pb/²⁰⁴Pb and ϵ_{Nd} and ²⁰⁸Pb/²⁰⁴Pb and ϵ_{Nd} . Summary statistics (means, variance, sample size) were used for source data input in the model as the source isotopic datasets were found to be neither consistently univariate nor multivariate normal for all PSAs (results of Shapiro-Wilk, Madia, Henze-Zirkler, and Royston statistical tests; see Supplementary Data Tables 2–5). All model iterations were run with no continuous effects, no concentration dependence, and no trophic enrichment factors (means and standard deviations equal to zero). Further, all models were run with residual error only and no process error. For iterations that evaluated source contributions over the whole 17JC record, 17JC sample age was used as a fixed effect for the mixture data. Dust contributions during distinct climate events of the past 30,000 years were obtained by grouping the model results of dust contributions over the entire core record *a posteriori* and calculating the average contribution of each source during each climate interval. MCMC chain length of each model iteration was optimized to reach convergence based on the results of post-run diagnostic tests offered in MixSIAR, the Gelman-Rubin and Geweke tests. For most models, we used the “very long” (chain length = 1 million) or “extreme” (chain length = 3 million) MCMC run options in MixSIAR. We report results from models for which all MCMC chains passed the Gelman–Rubin test (Gelman–Rubin reduction factor <1.05) and at least 2/3 chains passed the Geweke test (z-score = +/–1.96) (see Supplementary Data Tables 2–6).

Data availability

Source data are provided in the “Source Data File” in the supplementary material.

References

- Reimi, M. A. & Marcantonio, F. Constraints on the magnitude of the deglacial migration of the ITCZ in the Central Equatorial Pacific Ocean. *Earth Planet. Sci. Lett.* **453**, 1–8 (2016).
- Xie, R. C. & Marcantonio, F. Deglacial dust provenance changes in the Eastern Equatorial Pacific and implications for ITCZ movement. *Earth Planet. Sci. Lett.* **317–318**, 386–395 (2012).
- Reimi, M. A. et al. The penultimate glacial termination and variability of the pacific intertropical convergence zone. *Geophys. Res. Lett.* **46**, 4826–4835 (2019).
- Erhardt, A. M. et al. Assessing sedimentary detrital Pb isotopes as a dust tracer in the Pacific Ocean. *Paleoceanogr. Paleoclimatol.* **36**, e2020PA00414 (2021).
- Rea, D. K. The paleoclimatic record provided by eolian deposition in the deep sea: the geologic history of wind. *Rev. Geophys.* **32**, 159–195 (1994).
- Atwood, A. R. et al. Longitudinally variable responses of the ITCZ to a myriad of climate forcings. *Geophys. Res. Lett.* **47**, e2020GL088833 (2020).
- Schimmenti, D. et al. Insights into the deglacial variability of phytoplankton community structure in the eastern equatorial Pacific Ocean using [231Pa/230Th]xs and opal-carbonate fluxes. *Sci. Rep.* **12**, 22258 (2022).
- Kok, J. F. et al. Contribution of the world's main dust source regions to the global cycle of desert dust. *Atmos. Chem. Phys.* **21**, 8169–8193 (2021).
- Loveley, M. R. et al. Millennial-scale iron fertilization of the eastern equatorial Pacific over the past 100,000 years. *Nat. Geosci.* **10**, 760–764 (2017).
- Stock, B. et al. brianstock/MixSIAR 3.1.9. *Zenodo*, <https://doi.org/10.5281/zenodo.1209993> (2018).
- Stock, B. C. et al. Analyzing mixing systems using a new generation of Bayesian tracer mixing models. *PeerJ* **6**, e5096 (2018).
- Craigmile, P. F. EnvStats: an R package for environmental statistics by Steven P. Millard. *J. Agric. Biol. Environ. Stat.* **22**, 107–109 (2017).
- Oster, J. L. et al. North Atlantic meltwater during Heinrich Stadial 1 drives wetter climate with more atmospheric rivers in western North America. *Sci. Adv.* **9**, eadj2225 (2023).
- Hudson, A. M. et al. North-south dipole in winter hydroclimate in the western United States during the last deglaciation. *Sci. Rep.* **9**, 4826 (2019).
- Rasmussen, S. O. et al. A new Greenland ice core chronology for the last glacial termination. *J. Geophys. Res.* **111**, 2005JD006079 (2006).
- Kinsley, C. W. et al. Orbital- and millennial-scale variability in Northwest African dust emissions over the past 67,000 years. *Paleoceanogr. Paleoclimatol.* **37**, e2020PA004137 (2022).
- Tierney, J. E. et al. Rainfall regimes of the Green Sahara. *Sci. Adv.* **3**, e1601503 (2017).
- Marcantonio, F. et al. Deep equatorial Pacific Ocean oxygenation and atmospheric CO₂ over the last ice age. *Sci. Rep.* **10**, 6606 (2020).
- Luo, C. N. M. et al. Sensitivity study of meteorological parameters on mineral aerosol mobilization, transport, and distribution. *J. Geophys. Res.* **108**, 4447 (2003).
- Pichat, S. et al. Lead isotopes in the Eastern Equatorial Pacific record Quaternary migration of the South Westerlies. *Earth Planet. Sci. Lett.* **388**, 293–305 (2014).
- Gili, S. et al. Provenance of dust to Antarctica: a lead isotopic perspective. *Geophys. Res. Lett.* **43**, 2291e2298 (2016).
- Gili, S. et al. Glacial/interglacial changes of Southern Hemisphere wind circulation from the geochemistry of South American dust. *Earth Planet. Sci. Lett.* **469**, 98–109 (2017).
- Mamani, M. et al. Geochemical variations in igneous rocks of the Central Andean orocline (13 S to 18 S): Tracing crustal thickening and magma generation through time and space. *Geol. Soc. Am. Bull.* **122**, 162–182 (2010).
- Tapia, J. et al. Origin, distribution, and geochemistry of arsenic in the Altiplano-Puna plateau of Argentina, Bolivia, Chile, and Perú. *Sci. Total Environ.* **678**, 309–325 (2019).
- Lehnert, K. et al. A global geochemical database structure for rocks. *Geochem. Geophys. Geosyst.* **1**, 1–14 (2000).
- Guinoiseau, D. et al. Characterization of Saharan and Sahelian dust sources based on geochemical and radiogenic isotope signatures. *Quat. Sci. Rev.* **293**, 107729 (2022).

27. McGee, D. et al. Hemispherically asymmetric trade wind changes as signatures of past ITCZ shifts. *Quat. Sci. Rev.* **180**, 214–228 (2018).
28. Koutavas, A. & Lynch-Stieglitz, J. Variability of the marine ITCZ over the eastern Pacific during the past 30,000 years. In *The Hadley circulation: present, past and future* 347–369 (Springer, 2004).
29. Arbuszewski, J. A. et al. Meridional shifts of the Atlantic intertropical convergence zone since the Last Glacial Maximum. *Nat. Geosci.* **6**, 959–962 (2013).
30. Rowland, G. H. et al. The spatial distribution of aeolian dust and terrigenous fluxes in the tropical Atlantic Ocean since the Last Glacial Maximum. *Paleoceanogr. Paleoclimatol.* **36**, e2020PA004148 (2021).
31. Mosblech, N. A. S. et al. North Atlantic forcing of Amazonian precipitation during the last ice age. *Nat. Geosci.* **5**, 817–820 (2012).
32. McGee, D. et al. The magnitude, timing and abruptness of changes in North African dust deposition over the last 20,000 yr. *Earth Planet. Sci. Lett.* **371–372**, 163–176 (2013).
33. Demenocal, P. et al. Abrupt onset and termination of the African Humid Period: rapid climate responses to gradual insolation forcing. *Quat. Sci. Rev.* **19**, 347–361 (2000).
34. Thunell, R. C. et al. Calcite dissolution: an in situ study in the Panama Basin. *Science* **212**, 659–661 (1981).
35. Blauuw, M. et al. rbacon: Age-Depth Modelling using Bayesian Statistics. R package version 2.5.3 <https://CRAN.R-project.org/package=rbacon> (2021).
36. Wang, Y. J. et al. A high-resolution absolute-dated Late Pleistocene monsoon record from Hulu Cave, China. *Science* **294**, 2345 (2001).
37. Cisneros de León, A. et al. A history of violence: magma incubation, timing and tephra distribution of the Los Chocoyos supereruption (Atitlán Caldera, Guatemala). *J. Quat. Sci.* **36**, 169–179 (2021).
38. Yuan, H. et al. Evaluation of lead isotope compositions of NIST NBS 981 measured by thermal ionization mass spectrometer and multiple-collector inductively coupled plasma mass spectrometer. *Solid Earth Sci.* **1**, 74–78 (2016).
39. Tanaka, T. et al. JNd1-1: a neodymium isotopic reference in consistency with LaJolla neodymium. *Chem. Geol.* **168**, 279–281 (2000).
40. DePaolo, D. J. & Wasserburg, G. J. Nd isotopic variations and petrogenetic models. *Geophys. Res. Lett.* **3**, 249–252 (1976).
41. Prospero, J. M. et al. Environmental characterization of global sources of atmospheric soil dust identified with the nimbus 7 total ozone mapping spectrometer (toms) absorbing aerosol product: global sources of atmospheric soil dust. *Rev. Geophys.* **40**, 2-1–2–31 (2002).
42. Briceño-Zuluaga, F. et al. Paracas dust storms: Sources, trajectories and associated meteorological conditions. *Atmos. Environ.* **165**, 99–110 (2017).
43. Struve, T. et al. Systematic changes in circumpolar dust transport to the Subantarctic Pacific Ocean over the last two glacial cycles. *Proc. Natl Acad. Sci. USA* **119**, e2206085119 (2022).
44. Meyer, I. G. R. et al. (2011) Grain size control on Sr-Nd isotope provenance studies and impact on paleoclimate reconstructions: An example from deep-sea sediments offshore NW Africa. *Geochem. Geophys. Geosyst.* **12**, Q03005 (2011).
45. Longman, J. R. et al. Quantitative assessment of Pb sources in isotopic mixtures using a Bayesian mixing model. *Sci Rep* **8**, 6154 (2018).
46. Dietrich, M., Krekeler, M. P. S., Kousehlar, M. & Widom, E. Quantification of Pb pollution sources in complex urban environments through a multi-source isotope mixing model based on Pb isotopes in lichens and road sediment. *Environmental Pollution* **288**, 117815 (2021).
47. Lopez, A. M. et al. Lead geochemistry of sediments in Galveston Bay, Texas. *Environmental Advances* **4**, 100057 (2021).
48. Takahashi, T. et al. Climatological mean and decadal change in surface ocean pCO₂, and net sea-air CO₂ flux over the global oceans. *Deep Sea Res. Part II Topical Stud. Oceanogr.* **56**, 554–577 (2009).

Acknowledgements

This research was funded by NSF-OCE1803803 to F.M. Additional financial support to F.M. was provided by the generosity of the late R. Ken and Jane Williams.

Author contributions

D.E.S. and F.M. designed the study and wrote the manuscript. D.E.S. analyzed the samples and, together with M.R.S.H., performed the Bayesian MixSIAR mixing model analysis. D.E.S., F.M., M.R.S.H., and M.W.S. interpreted the data and contributed to the manuscript.

Competing interests

The authors declare no competing interests.

Additional information

Supplementary information The online version contains supplementary material available at <https://doi.org/10.1038/s41467-025-60773-7>.

Correspondence and requests for materials should be addressed to Franco Marcantonio.

Peer review information *Nature Communications* thanks Aloys Bory and the other, anonymous, reviewer(s) for their contribution to the peer review of this work. A peer review file is available.

Reprints and permissions information is available at <http://www.nature.com/reprints>

Publisher's note Springer Nature remains neutral with regard to jurisdictional claims in published maps and institutional affiliations.

Open Access This article is licensed under a Creative Commons Attribution-NonCommercial-NoDerivatives 4.0 International License, which permits any non-commercial use, sharing, distribution and reproduction in any medium or format, as long as you give appropriate credit to the original author(s) and the source, provide a link to the Creative Commons licence, and indicate if you modified the licensed material. You do not have permission under this licence to share adapted material derived from this article or parts of it. The images or other third party material in this article are included in the article's Creative Commons licence, unless indicated otherwise in a credit line to the material. If material is not included in the article's Creative Commons licence and your intended use is not permitted by statutory regulation or exceeds the permitted use, you will need to obtain permission directly from the copyright holder. To view a copy of this licence, visit <http://creativecommons.org/licenses/by-nc-nd/4.0/>.

© The Author(s) 2025